

# Spatially Resolved Measurements of Argon Metastable ( $1s_5$ ) Density in a High Pressure Microdischarge Using Diode Laser Absorption Spectroscopy

Sergey G. Belostotskiy, Vincent M. Donnelly, Demetre J. Economou, and Nader Sadeghi

**Abstract**—Tunable diode laser absorption spectroscopy was employed to measure the spatially resolved density of argon metastables ( $1s_5$ ) in a high-pressure direct-current argon microdischarge. Analysis of absorption lineshapes provided the gas temperature. The metastable density peaked near the cathode and decayed rapidly in the bulk plasma. The metastable density increased with increasing pressure but decreased with increasing discharge current. Neutral gas heating and the resulting drop in gas density were responsible for the metastable density decrease with increasing current.

**Index Terms**—Argon microdischarge, atmospheric pressure microplasma, diode laser absorption spectroscopy, metastable density, plasma diagnostics.

## I. INTRODUCTION

HIGH-PRESSURE (hundreds of torr) microdischarges have attracted much attention recently [1]–[13], due to numerous applications or potential applications in plasma display panels, excimer radiation sources, sensors, microreactors, materials treatment and modification, sterilization, plasma surgery, etc.

Microdischarge diagnostics are indispensable for better understanding microdischarge physics and optimizing device performance. However, the application of conventional diagnostics (e.g., Langmuir probes) is complicated due to the small size (hundreds of micrometers), high operating pressure, and high power density (tens to hundreds of kilowatts per cubic centimeter) of microdischarges. In contrast, nonintrusive optical diagnostic methods are convenient for characterization of microdischarges. We have applied Stark emission spectroscopy, Raman scattering, and Thomson scattering to measure electric fields, gas temperatures, and charged and neutral species den-

sities in slotted direct-current (dc) microdischarges [6], [10], [12]. Thomson scattering measurements in an argon microdischarge [12] revealed a rather high electron density ( $n_e = (6 \pm 3) \times 10^{13} \text{ cm}^{-3}$ ) at a relatively low electron temperature ( $T_e = 0.9 \pm 0.3 \text{ eV}$ ) in the bulk plasma.

Stepwise ionization through the metastable states is known to be an important mechanism in argon and other rare gas plasmas, particularly when the electron temperature is low [14]. Thus, the metastable argon ( $\text{Ar}^*$ ) density might be an important parameter that affects the microdischarge properties, making direct measurement of  $\text{Ar}^*$  highly desirable. Measurements of  $\text{Ar}^*$  in various types of microdischarges were reported by several groups (see, e.g., [13] and [15]). Most of these measurements were not spatially resolved, however. In this paper, spatially resolved profiles of  $\text{Ar}(1s_5)$  (lowest metastable state) density were measured using tunable diode laser absorption spectroscopy.

## II. EXPERIMENTAL DETAILS

The apparatus used for tunable diode laser absorption spectroscopy is shown schematically in Fig. 1. A parallel-plate slot-type microdischarge [11], [12] was sustained between two rectangular ( $5 \text{ mm} \times 0.5 \text{ mm}$ ) molybdenum electrodes, spaced  $300 \mu\text{m}$  apart. An external cavity diode laser (ECDL) in the Littman configuration (LION—Sacher Lasertechnik, Marburg, Germany) was used as the light source. The width of the laser line ( $< 10 \text{ MHz}$ ) was much smaller than the typical bandwidth of the absorption line ( $> 1 \text{ GHz}$ ). Therefore, the absorption profile was recorded, without using a high-resolution spectrometer, by scanning the laser frequency across the absorption line. The laser frequency was finely and accurately scanned by changing the voltage on the piezoelectric element that moved one of the cavity mirrors. The laser beam from the ECDL passed through a beam splitter. Part of the beam was guided to a Fabry–Perot interferometer (1-GHz free spectral range) to perform *in situ* calibration of the laser frequency. The rest of the beam was attenuated to  $< 100 \mu\text{W}$  by a set of neutral density filters, directed through the interelectrode space of the microdischarge, and then through an aperture. The aperture suppressed emission from the plasma by reducing the collection solid angle. When desired, plasma emission was recorded simply by increasing the size of the aperture. A set of mirrors was used to magnify (11X) and image the laser light on a linear CCD array (Thorlabs

Manuscript received December 3, 2008; revised February 9, 2009. First published April 7, 2009; current version published June 10, 2009. This work was supported in part by the Department of Energy (DE-FG02-03ER54713), by the University of Houston GEAR program, and by the Texas Advanced Research Program.

S. G. Belostotskiy, V. M. Donnelly, and D. J. Economou are with the Plasma Processing Laboratory, Department of Chemical and Biomolecular Engineering, University of Houston, Houston, TX 77204-4004 USA (e-mail: vmdonnelly@uh.edu; economou@uh.edu).

N. Sadeghi is with the Laboratoire de Spectrométrie Physique (UMR C5588), Université J. Fourier de Grenoble, 38402 Saint-Martin d'Hères Cedex, France.

Color versions of one or more of the figures in this paper are available online at <http://ieeexplore.ieee.org>.

Digital Object Identifier 10.1109/TPS.2009.2015949

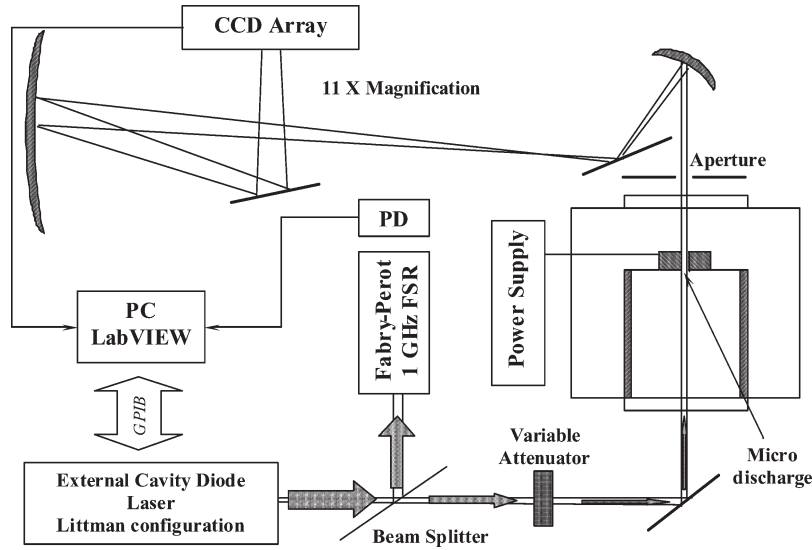
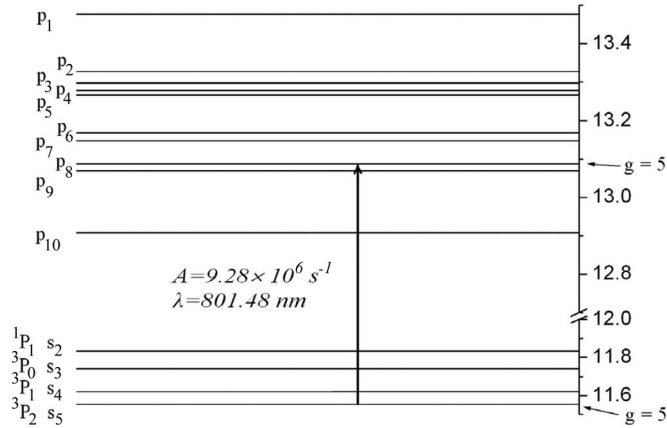


Fig. 1. Experimental setup for tunable diode laser absorption spectroscopy.


 Fig. 2. Diagram of the argon  $3p^5 4s$  and  $3p^5 4p$  states and the transition used in the experiment.

LC1-USB, Karlsfeld, Germany), which allowed spatially resolved (across the electrodes) measurement in a single acquisition. The experiment was controlled by LabVIEW software (National Instruments, Austin, TX).

To avoid possible long-term drift of laser power or frequency, reference ( $I_0$ ) and absorption ( $I$ ) intensities were collected by pulsing the plasma ( $\sim 1$  Hz) and recording  $I_0$  with plasma off, and  $I$  with plasma on, for each laser frequency. Such a procedure is important for spatially resolved measurements, since the spatial distribution of laser intensity across the beam may vary with laser frequency. The transition from the lowest metastable state  $\text{Ar}(2p_8) \leftarrow \text{Ar}(1s_5, ^3P_2)$  (Einstein A coefficient =  $9.28 \cdot 10^6 \text{ s}^{-1}$  [16], [17]) at  $\lambda = 801.48 \text{ nm}$  was used for absorption measurements (see Fig. 2).

### III. ABSORPTION SPECTROSCOPY

Absorption spectroscopy is based on Beer–Lambert’s law [18]

$$\ln \left( \frac{I_0(\nu)}{I(\nu)} \right) = \int_{-\infty}^{\infty} k(\nu, x) \cdot dx \quad (1)$$

where  $I_0(\nu)$  is a reference intensity at frequency  $\nu$  (in this experiment with the plasma off),  $I(\nu)$  is the intensity after passing through the absorbing medium (plasma on), and  $k(\nu, x)$  is the absorption coefficient per unit length, given by

$$k(\nu, x) = \frac{g_u}{g_l} \cdot \lambda_0^2 \cdot \frac{A_{ul}}{8\pi} \cdot \left( N_l(x) - \frac{g_l}{g_u} \cdot N_u(x) \right) \cdot f(\nu) \quad (2)$$

where  $g_u$  and  $g_l$  are the statistical weights of the upper and lower levels, respectively,  $\lambda_0$  is the central wavelength of the transition,  $A_{ul}$  is the Einstein’s coefficient for spontaneous emission from the upper to the lower level,  $N_u(x)$  and  $N_l(x)$  are the densities of the upper and lower levels, respectively, and  $f(\nu)$  is a normalized function ( $\int_{-\infty}^{\infty} f(\nu) \cdot d\nu = 1$ ), representing the absorption lineshape.

For most electronic transitions, the energy gap between the upper and lower levels is large compared to the gas temperature ( $E_u - E_l \gg k_b \cdot T_g$ , where  $k_b$  is the Boltzmann constant), so that the population of the upper level can be neglected ( $N_u \ll N_l$ ). Then, averaging (1) with respect to position along the beam path, one obtains

$$\ln \left( \frac{I_0(\nu)}{I(\nu)} \right) = \frac{g_u}{g_l} \cdot \lambda_0^2 \cdot \frac{A_{ul}}{8\pi} \cdot \langle N_l \rangle \cdot l_{\text{eff}} \cdot f(\nu) \quad (3)$$

where  $\langle N_l \rangle$  is the line-averaged density of  $\text{Ar}(1s_5)$  and  $l_{\text{eff}}$  is an effective absorption length. To accurately determine the absorption length, one needs to know the spatial profile of the absorbing species along the direction of the laser beam. It was assumed that due to the relatively low diffusion coefficient of  $\text{Ar}(1s_5)$  atoms at high neutral gas density ( $DN \cong 1.8 \times 10^{18} \text{ molecule} \cdot \text{cm}^{-1} \cdot \text{s}^{-1}$ ) and their fast loss by electron impact reactions (see below), the metastables were confined in the place where they were produced, i.e., between the electrodes. Thus, the length of the electrodes in the direction of propagation of the laser beam (0.5 mm) was taken as the effective length  $l_{\text{eff}}$ .

The area under the absorption curve (integration of (3) with respect to frequency  $\nu$ ) provides the line-averaged density of absorbing species. Analysis of the lineshape can provide the gas temperature. The absorption lineshape can be described by a Voigt function, i.e., a convolution of Lorentzian and Gaussian functions [20]

$$f_V(\nu) = \frac{1}{\pi^{3/2}} \cdot \frac{\Delta\nu_L}{4 \cdot \Delta\nu_D^2} \int_{-\infty}^{\infty} \frac{\exp(-t^2)}{\left(\frac{\nu-\nu_0}{\sqrt{2} \cdot \Delta\nu_D} - t\right)^2 + \left(\frac{\Delta\nu_L}{2 \cdot \sqrt{2} \cdot \Delta\nu_D}\right)^2} \cdot dt. \quad (4)$$

In (4),  $\Delta\nu_D$  is the width (standard deviation) of the Gaussian component, caused by Doppler broadening

$$\Delta\nu_D = \frac{1}{\lambda_0} \cdot \sqrt{\frac{k_b \cdot T}{M_{\text{Ar}}}} \quad (5)$$

where  $T$  is the temperature of the absorbing species (assumed equal to the gas temperature  $T_g$ ) and  $M$  is the mass of the absorbing species (the mass of argon atoms in this case). The FWHM of the Lorentzian component  $\Delta\nu_L$  is governed by four broadening mechanisms: natural, power, Stark, and pressure broadening.

For the transition used in this paper, the natural width is relatively small ( $(1/2\pi\tau) \cong 5.2$  MHz with  $\tau = 30.6$  ns [17]). To avoid power broadening, the power of the laser beam was attenuated, so that the saturation parameter [18] was smaller than unity,  $S \ll 1$ . According to the study in [12], the electron density in this type of microdischarge is at most  $\sim 10^{14}$  cm $^{-3}$ , corresponding to a Stark width of  $\sim 10$  MHz [21]. For the transition and pressure range used here, pressure broadening is typically  $> 0.5$  GHz, making it the main mechanism responsible for the Lorentzian component of the lineshape.

From the theory of pressure broadening [22]–[24], one obtains the following expression for the Lorentzian FWHM:

$$\Delta\nu_L = 2\gamma_0 \cdot \left(\frac{T_g}{T_0}\right)^{0.3} \cdot N = 2\gamma_0 \cdot \left(\frac{T_g}{T_0}\right)^{0.3} \cdot \frac{P}{k_b \cdot T_g} \quad (6)$$

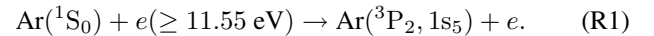
where  $P$  is the gas pressure and  $\gamma_0$  is the reduced width at reference temperature  $T_0$ . Equation (6) is valid for gas temperatures below  $\sim 2000$  K [24]. The value  $\gamma_0 = 8.69 \cdot 10^{-19}$  GHz  $\cdot$  cm $^3$  measured at  $T_0 = 1130$  K was taken from the work of Copley and Camm [25]. The gas temperature was extracted by fitting experimental lineshapes to (4) using the gas temperature as the only fitting parameter.

#### IV. RESULTS AND DISCUSSION

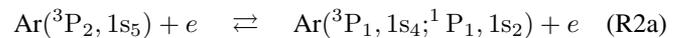
Fig. 3 shows the profiles of transmitted laser intensity as a function of interelectrode distance and laser frequency, with the plasma on ( $I$ , Fig. 3(a), linear scale) and off ( $I_0$ , Fig. 3(b), linear scale). Fig. 3(c) shows the ratio  $I_0/I$  on a logarithmic scale. For a given microdischarge operating condition, one can obtain spatially resolved profiles of the argon metastable density (Fig. 4) by integrating the profile of Fig. 3(c) with respect to laser frequency at different spatial locations.

Fig. 4 shows that the Ar $^*$  density profile peaks near the cathode and decays rapidly toward the bulk plasma. Such behavior is consistent with the properties of the cathode sheath and negative glow, where most of metastable production occurs. The excitation threshold for Ar( $1s_5$ ) is 11.55 eV. Therefore, high-energy electrons are needed to excite argon atoms to metastable states. These are secondary electrons emitted at the cathode surface as a result of bombardment by ions as well as by photon and metastable atom bombardment. The electron “temperature” reaches a maximum near the cathode sheath edge. On the other hand, the electron temperature in the bulk plasma is very low ( $\sim 1$  eV), yielding very low rates of metastable production. In addition, as pressure increases, the metastable density gradient becomes stronger and the profile moves closer to the cathode [Fig. 4(c)] since the penetration depth of the secondaries diminishes with increasing pressure. This is shown more clearly (Fig. 5) by the spatially resolved optical emission of the Ar $^+$  line at 427.75 nm ( $3s^2 3p^4(^1D)4p \rightarrow 3s^2 3p^4(^1D)4s$ ). The upper level of this line is 37.1 eV above the ground-state argon atom. The peak emission shifts toward the cathode as pressure increases.

Furthermore, the peak argon metastable density increases with increasing pressure [Fig. 4(c)] but decreases with increasing discharge current [Figs. 4(a) and (b)]. Such behavior of metastable density with current seemed curious, since metastable atoms are produced by electron impact excitation. To understand the metastable density behavior, one should examine the mechanisms of metastable production and loss. The main Ar( $1s_5$ ) production mechanism is direct electron impact excitation from the ground state



In low-pressure plasmas, a major metastable loss mechanism is electron quenching to a nearby resonant state (reaction (R2a), rate constant  $k_2 \approx 2 \cdot 10^{-7}$  cm $^3$ /s [26]), followed by fast radiative decay to the ground state [reaction (R2b)].



In high-pressure plasmas, however, photons emitted by radiative relaxation of the resonant state are reabsorbed (radiation trapping) by ground-state atoms [reverse of reaction (R2b)]. For example, at a pressure of 100 torr and gas temperature of 1000 K, the “effective” absorption length was estimated to be  $L_{\text{abs}} \approx 70$  nm which is much smaller than the plasma length. The resonant state formed as a result of the reverse of reaction (R2b) can then reform metastables by the reverse of reaction (R2a) (rate constant  $k_{-2} \approx 3.5 \cdot 10^{-7}$  cm $^3$ /s [26]). In essence, radiation trapping leads to an *effective* rate of metastable quenching in reaction (R2a) that is much slower than the inherent reaction rate.

Other loss mechanisms of Ar( $1s_5$ ) metastables are electron impact ionization (R3), electron impact excitation to higher electronic levels followed by collisional relaxation to the ground state (R4), metastable pooling (R5), two-body

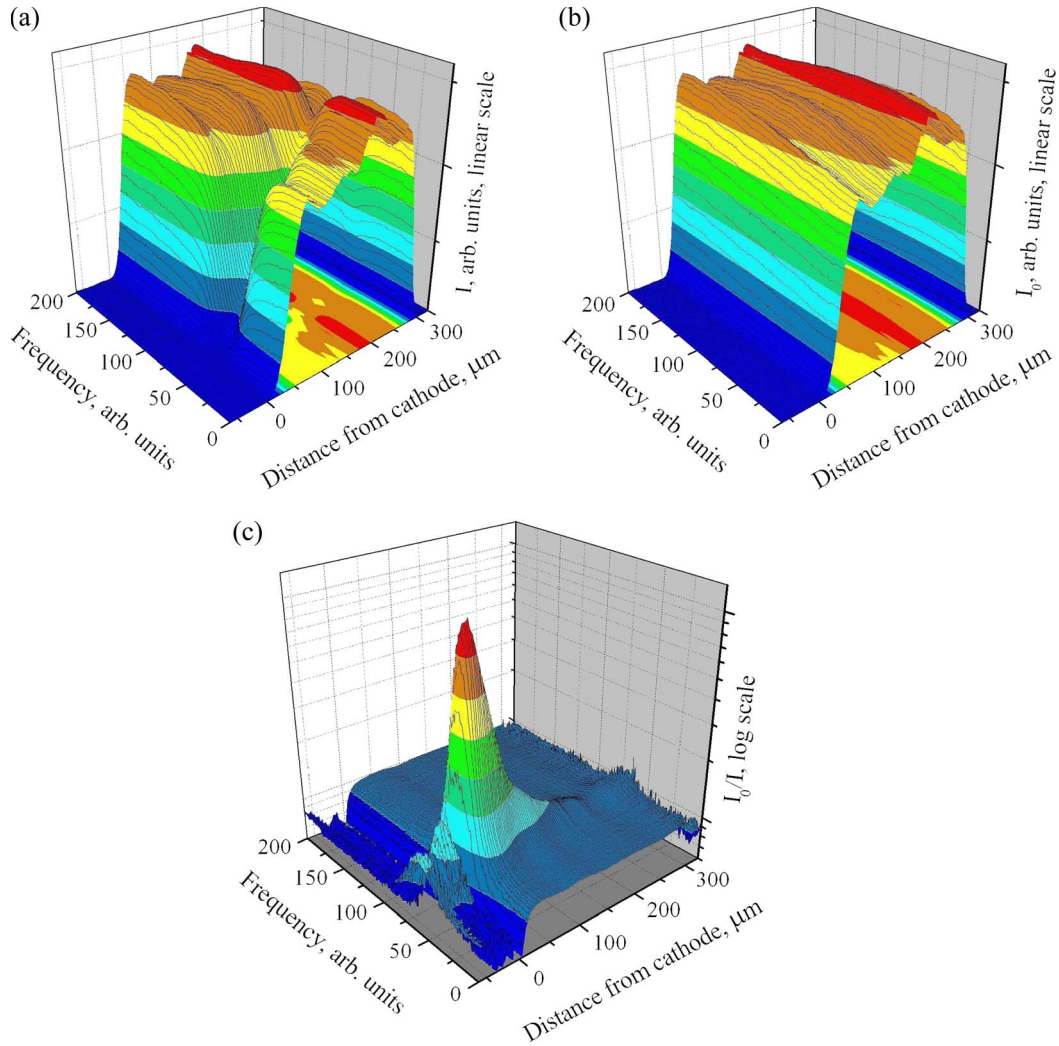
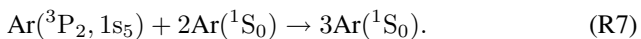
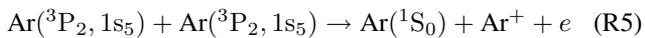
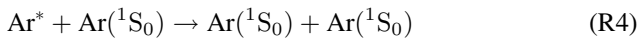
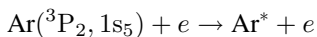
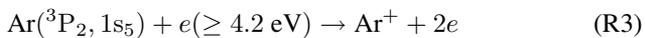


Fig. 3. Profiles of transmitted laser intensity as a function of interelectrode distance and laser frequency: (a) Intensity  $I$  for plasma-on (linear scale) state; (b) intensity  $I_0$  for plasma-off (linear scale) state; and (c) ratio  $I_0/I$  (logarithmic scale).

collisional quenching (R6), three-body collisional quenching (R7), and diffusion [27]



Estimates of the contribution of each of these loss processes were performed. The rate constants for reactions (R5)–(R7) were taken from [27]. For reaction (R3), the ionization cross section [28] was convoluted with a Maxwellian electron energy distribution function (EEDF). The cross sections [29], [30] for reaction (R4) have lower threshold and higher peak value than reaction (R3). Hence, electron impact excitation of high electronic levels of Ar occurs faster than ionization. However, most of the excited atoms decay back to the metastable states through radiative relaxation.

Electron impact ionization [reaction (R3)] was found to be the dominant loss mechanism of metastables near the sheath edge ( $S_{q3} > 10^6 \text{ s}^{-1}$ ; for  $T_e > 1.6 \text{ eV}$ , an electron temperature that can easily be achieved in that region of the discharge). The rate of metastable loss through diffusion is negligibly small ( $S_D \sim 10^3 \text{ s}^{-1}$ ). We should mention here that at higher pressures ( $> 300 \text{ torr}$ ) and in the bulk plasma, where both electron temperature and gas temperature drop, three-body collisional quenching (R7) becomes important. For example, at 300 torr and 700 K,  $S_{q7} \sim 2 \cdot 10^5 \text{ s}^{-1}$ . Thus, this process only enhances the decay of the metastables toward the bulk plasma. The metastable pooling reaction (R5) is quadratic with respect to metastable density. Near the sheath edge, metastable loss due to this reaction ( $S_{q5} \sim 10^5 \text{ s}^{-1}$ ) is still slower than electron impact ionization (R3), and in the bulk, it is negligible due to the very low metastable density.

Equating production and loss at steady state, one obtains an expression for the  $\text{Ar}(1s_5)$  density

$$[\text{Ar}(1s_5)] = \frac{\langle \sigma_{\text{ex}} \cdot \nu \rangle_{\text{EEDF}} \cdot n_e}{\langle \sigma_i \cdot \nu \rangle_{\text{EEDF}} \cdot n_e} \cdot [\text{Ar}] = \frac{\langle \sigma_{\text{ex}} \cdot \nu \rangle_{\text{EEDF}}}{\langle \sigma_i \cdot \nu \rangle_{\text{EEDF}}} \cdot \frac{P}{k_b T_g} \quad (7)$$

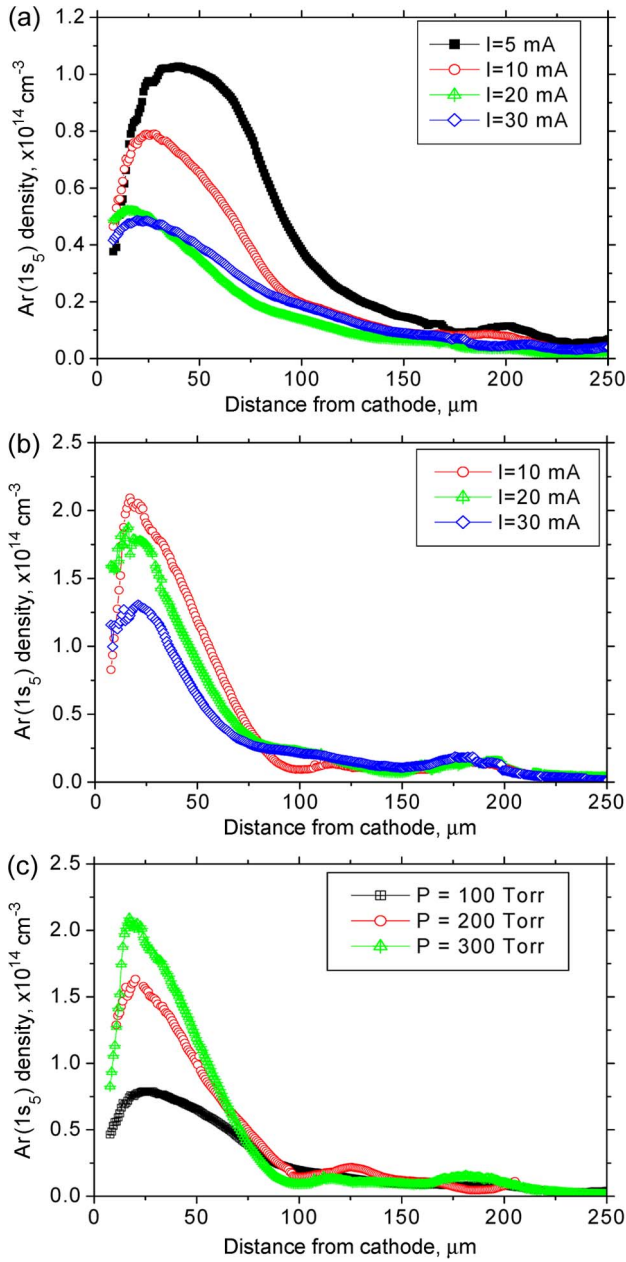


Fig. 4. Spatial profiles of argon metastable density (a) at 100 torr and different currents, (b) at 300 torr and different currents, and (c) at 10 mA and different pressures.

where  $[Ar(1s_5)]$  and  $[Ar]$  are the densities of argon metastables and ground-state atoms, respectively,  $\langle\sigma_{ex} \cdot \nu\rangle_{EEDF}$  is the rate coefficient of electron impact excitation [reaction (R1)], and  $\langle\sigma_i \cdot \nu\rangle_{EEDF}$  is the rate coefficient of electron impact ionization from the  $Ar(1s_5)$  state [reaction (R3)]. It should be noted that both coefficients depend strongly on the EEDF. However, their ratio  $\langle\sigma_{ex} \cdot \nu\rangle_{EEDF} / \langle\sigma_i \cdot \nu\rangle_{EEDF}$  should have a much weaker dependence on the EEDF, i.e., a weak dependence on either pressure or current. Thus, knowledge of the values of the rate coefficients is not necessary to analyze trends in the metastable density. To obtain an order-of-magnitude estimate, the excitation and ionization cross sections [28], [31] were convoluted with a Maxwellian EEDF. It was found that an electron temperature of  $T_e \sim 1.5 \text{ eV}$  (this can be easily achieved near the

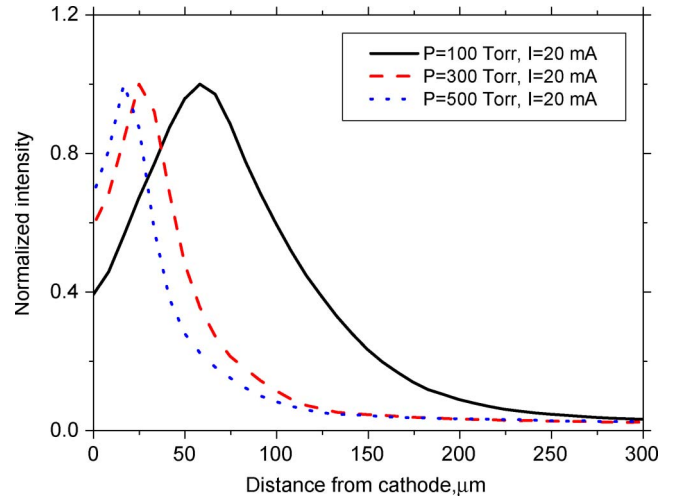


Fig. 5.  $Ar^+$  emission at  $\lambda = 427.75 \text{ nm}$  as a function of distance from the cathode. The energy of the emitting level is 37.1 eV above the ground state.

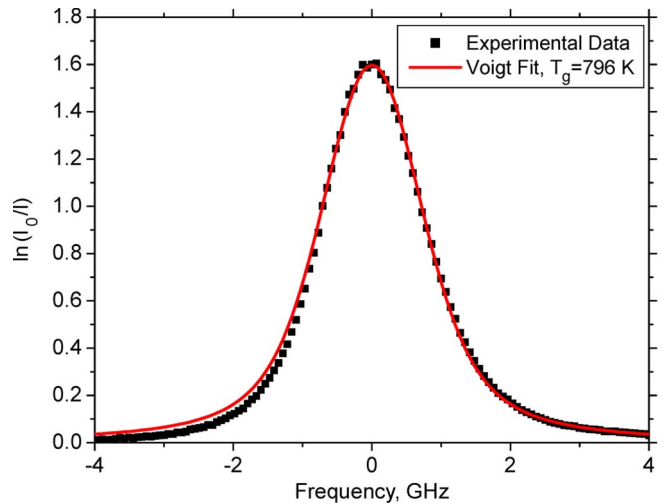


Fig. 6. Example of absorption profile fit:  $P = 100 \text{ torr}; I = 20 \text{ mA}$ .

sheath edge) would be high enough to produce the metastable density observed in the experiments ( $\sim 10^{14} \text{ cm}^{-3}$ ).

Equation (7) predicts that the argon metastable density should increase with pressure, as observed experimentally [Fig. 4(c)]. In addition, according to this equation, there is no explicit dependence of metastable density on electron density (discharge current). However, increasing discharge current would be expected to cause the gas temperature to increase, and this could explain the decrease in Ar metastable density at high currents. In fact, (7) shows that, for a constant pressure, the argon metastable density should decrease inversely proportionally to gas temperature. To test this dependence, the gas temperature was extracted by analyzing the absorption lineshapes. Experimental profiles were fit to a Voigt function (4) with  $T_g$  as the fitting parameter. An example of a lineshape fit at a pressure  $P = 100 \text{ torr}$  and current  $I = 20 \text{ mA}$  is shown in Fig. 6. Here, the  $x$ -axis represents frequency, relative to the line center. Absolute calibration (e.g., with a low-pressure argon discharge) of the frequency was not done in this paper.

Based on fits such as shown in Fig. 6, the gas temperature was determined. A plot of gas temperature and peak  $Ar(1s_5)$

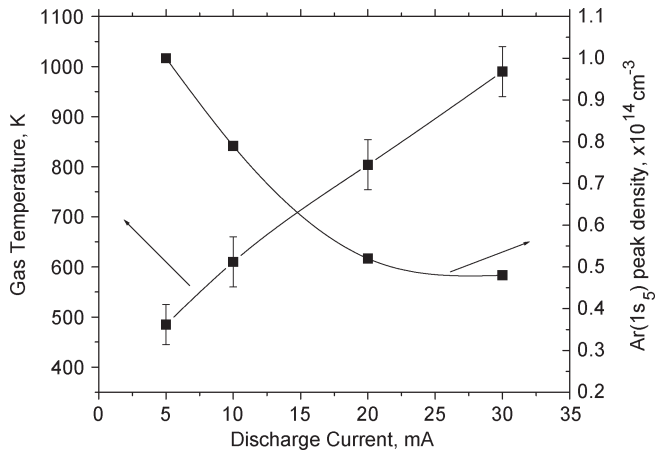


Fig. 7. Gas temperature and peak Ar( $1s_5$ ) density versus discharge current at  $P = 100$  torr.

density versus discharge current is presented in Fig. 7 for  $P = 100$  torr. Gas temperature measurements were performed at the spatial location of the peak argon metastable density. The gas temperature increases from  $\sim 500$  K at 5 mA to  $\sim 1000$  K at 30 mA, corresponding to a decrease of the peak argon metastable density from  $\sim 10^{14} \text{ cm}^{-3}$  to  $0.5 \times 10^{14} \text{ cm}^{-3}$  in agreement with (7). Therefore, neutral gas heating and the resulting drop in neutral gas density can explain the decrease of argon metastable density with increasing current.

It should be noted that gas pressure contributes not only to profile broadening but also to a shift of the absorption line. This pressure shift can be described by [24]

$$\Delta\nu_{\text{Shift}} = -\beta_0 \cdot \left(\frac{T_g}{T_0}\right)^{0.3} \cdot N = -\beta_0 \cdot \left(\frac{T_g}{T_0}\right)^{0.3} \cdot \frac{P}{k_b \cdot T_g} \quad (8)$$

where  $\beta_0$  is the reduced shift at a reference temperature  $T_0$ . The value  $\beta_0 = 2.79 \cdot 10^{-19} \text{ GHz} \cdot \text{cm}^3$  at the temperature  $T_0 = 1130$  K was again taken from the work of Copley and Camm [25]. It turns out that at  $P = 100$  torr, the frequency shift ( $< 0.5$  GHz) is small compared to the Doppler width. However, at  $P = 300$  torr, the frequency shift is of the same order as the Doppler width. Thus, any temperature gradients along the laser beam propagation direction would result not only in superposition of lines with various widths but also in distortion of the absorption profile (e.g., the profile becomes asymmetric). Therefore, fitting of absorption lineshapes at higher pressures is problematic and was not done.

Another source of distortion of the lineshape may be due to slight deflection of the laser beam in the plasma. Temperature gradients cause gradients in the refractive index, which, in turn, cause a slight deflection of the beam when the plasma is on. Since the absorption profile is obtained from the ratio of the laser profile when plasma is on and off, a slight spatial shift of the laser beam may result in distortion of the absorption lines, adding a baseline to the experimental profiles. This baseline would vary from cathode to anode because of the temperature gradient across the electrodes [6], [11]. Such distortions may be reduced if the spatial profile of the laser beam is "smooth"

enough such that slight deflection does not cause a considerable baseline shift.

## V. CONCLUSION

Tunable diode laser absorption spectroscopy was employed to measure the spatially resolved density of argon metastables Ar( $1s_5$ ) in high-pressure dc argon microdischarges. The argon metastable density peaked near the cathode and decayed rapidly toward the bulk plasma. The peak metastable density increased with increasing pressure but decreased with increasing discharge current. Analysis of Ar( $1s_5$ ) production and loss mechanisms revealed that the metastable density should be proportional to the density of the ground-state atoms. Therefore, the metastable density should increase proportionally to pressure and inversely proportionally to gas temperature. Furthermore, analysis of absorption lineshapes was performed to study the effect of discharge current on gas temperature. The main mechanisms responsible for absorption line broadening were Doppler broadening and pressure broadening. By fitting the absorption lineshapes to Voigt functions, the gas temperature was extracted as the fitting parameter. The gas temperature increased with discharge current, resulting in neutral gas depletion and hence to the observed decrease of Ar( $1s_5$ ) density with current.

## REFERENCES

- [1] K. H. Becker, K. H. Schoenbach, and J. G. Eden, "Microplasmas and applications," *J. Phys. D, Appl. Phys.*, vol. 39, no. 3, pp. R55–R70, Feb. 2006.
- [2] M. Kushner, "Modelling of microdischarge devices: Plasma and gas dynamics," *J. Phys. D, Appl. Phys.*, vol. 38, no. 11, pp. 1633–1643, Jun. 2005.
- [3] U. Kogelschatz, "Atmospheric-pressure plasma technology," *Plasma Phys. Control. Fusion*, vol. 46, no. 12B, pp. B63–B75, Dec. 2004.
- [4] J. P. Boeuf, "Plasma display panels: Physics, recent developments and key issues," *J. Phys. D, Appl. Phys.*, vol. 36, no. 6, pp. R53–R79, Mar. 2003.
- [5] K. Tachibana, S. Kawai, H. Asai, N. Kikuchi, and S. Sakamoto, "Characteristics of Ne–Xe microplasma in unit discharge cell of plasma display panel equipped with counter sustain electrodes and auxiliary electrodes," *J. Phys. D, Appl. Phys.*, vol. 38, no. 11, pp. 1739–1749, Jun. 2005.
- [6] Q. Wang, I. Koleva, V. M. Donnelly, and D. J. Economou, "Spatially resolved diagnostics of an atmospheric pressure direct current helium microplasma," *J. Phys. D, Appl. Phys.*, vol. 38, no. 11, pp. 1690–1697, Jun. 2005.
- [7] Y. Noguchi, A. Matsuoka, M. D. Bowden, K. Uchino, and K. Muraoka, "Measurements of electron temperature and density of a micro-discharge plasma using laser Thomson scattering," *Jpn. J. Appl. Phys.*, vol. 40, no. 1, pp. 326–329, Jan. 2001.
- [8] A. Kono and K. Iwamoto, "High-spatial-resolution multichannel Thomson scattering measurements for atmospheric pressure microdischarge," *Jpn. J. Appl. Phys.*, vol. 43, no. 8A, pp. L1 010–L1 013, Jul. 2004.
- [9] S. Hassaballa, M. Yakushiji, Y.-K. Kim, K. Tomita, K. Uchino, and K. Muraoka, "Two-dimensional structure of PDP micro-discharge plasmas obtained using laser Thomson scattering," *IEEE Trans. Plasma Sci.*, vol. 32, no. 1, pp. 127–134, Feb. 2004.
- [10] S. G. Belostotskiy, V. M. Donnelly, and D. J. Economou, "Influence of gas heating on high pressure dc microdischarge  $I$ – $V$  characteristics," *Plasma Sources Sci. Technol.*, vol. 17, no. 4, p. 045 018, Nov. 2008.
- [11] S. G. Belostotskiy, Q. Wang, V. M. Donnelly, D. J. Economou, and N. Sadeghi, "Three-dimensional gas temperature measurements in atmospheric pressure microdischarges using Raman scattering," *Appl. Phys. Lett.*, vol. 89, no. 25, p. 251 503, Dec. 2006.
- [12] S. G. Belostotskiy, R. Khandelwal, Q. Wang, V. M. Donnelly, D. J. Economou, and N. Sadeghi, "Measurement of electron temperature and density in an argon microdischarge by laser Thomson scattering," *Appl. Phys. Lett.*, vol. 92, no. 22, p. 221 507, Jun. 2008.

- [13] C. Penache, M. Miclea, A. Brauning-Demian, O. Hohn, S. Schossler, T. Jahnke, K. Niemax, and H. Schmidt-Bocking, "Characterization of a high-pressure microdischarge using diode laser atomic absorption spectroscopy," *Plasma Sources Sci. Technol.*, vol. 11, no. 4, pp. 476–483, Nov. 2002.
- [14] D. P. Lymberopoulos and D. J. Economou, "Fluid simulations of glow discharges: Effect of metastable atoms in argon," *J. Appl. Phys.*, vol. 73, no. 8, pp. 3668–3679, Apr. 1993.
- [15] L. Latrasse, N. Sadeghi, A. Lacoste, A. Bes, and J. Pelletier, "Characterization of high density matrix microwave argon plasmas by laser absorption and electric probe diagnostics," *J. Phys. D, Appl. Phys.*, vol. 40, no. 17, pp. 5177–5186, Sep. 2007.
- [16] *NIST Atomic Spectra Database*. [Online]. Available: <http://physics.nist.gov/PhysRefData/ASD/index.html>
- [17] W. L. Wiese, J. W. Brault, K. Danzmann, V. Helbig, and M. Kock, "Unified set of atomic transition probabilities for neutral argon," *Phys. Rev. A, Gen. Phys.*, vol. 39, no. 5, pp. 2461–2471, Mar. 1989.
- [18] N. Sadeghi, "Molecular spectroscopy techniques applied for processing plasma diagnostics," *J. Plasma Fusion Res.*, vol. 80, no. 9, pp. 767–776, Sep. 2004.
- [19] J. H. Kolts and D. W. Setser, "Decay rates of  $\text{Ar}(4s, ^3P_2)$ ,  $\text{Ar}(4s', ^3P_0)$ ,  $\text{Kr}(5s, ^3P_2)$ , and  $\text{Xe}(6s, ^3P_2)$  atoms in argon," *J. Chem. Phys.*, vol. 68, no. 11, pp. 4848–4859, Jun. 1978.
- [20] A. Corney, *Atomic and Laser Spectroscopy*. Oxford, U.K.: Oxford Science, 1988.
- [21] N. Konjevic, A. Lesage, J. R. Fuhra, and W. L. Wiese, "Experimental stark widths and shifts for spectral lines of neutral and ionized atoms (A critical review of selected data for the period 1989 through 2000)," *J. Phys. Chem. Ref. Data*, vol. 31, no. 3, pp. 819–927, Sep. 2002.
- [22] E. Lindholm, *Arkiv. Mat. Astron. Fys.*, vol. 32A, no. 17, p. 1, 1945.
- [23] H. M. Foley, "The pressure broadening of spectral lines," *Phys. Rev.*, vol. 69, no. 11/12, pp. 616–628, Jun. 1946.
- [24] P. S. Moussounda and P. Ranson, "Pressure broadening of argon lines emitted by a high-pressure microwave discharge (surfatron)," *J. Phys. B: At. Mol. Phys.*, vol. 20, no. 5, pp. 949–961, Mar. 1987.
- [25] G. H. Copley and D. M. Camm, "Pressure broadening and shift of argon emission lines," *J. Quant. Spectrosc. Radiat. Transf.*, vol. 14, no. 9, pp. 899–907, Sep. 1974.
- [26] C. M. Ferreira, J. Loureiro, and A. Ricard, "Populations in the metastable and the resonance levels of argon and stepwise ionization effects in a low-pressure argon positive column," *J. Appl. Phys.*, vol. 57, no. 1, pp. 82–90, Jan. 1985.
- [27] A. Bogaerts and R. Gijbels, "Modeling of metastable argon atoms in a direct-current glow discharge," *Phys. Rev. A, Gen. Phys.*, vol. 52, no. 5, pp. 3743–3751, Nov. 1995.
- [28] E. J. McGuire, "Scaled electron ionization cross sections in the Born approximation for atoms with  $55 \leq Z \leq 102$ ," *Phys. Rev. A, Gen. Phys.*, vol. 20, no. 2, pp. 445–456, Aug. 1979.
- [29] H. A. Hyman, "Electron-impact excitation of metastable argon and krypton," *Phys. Rev. A, Gen. Phys.*, vol. 18, no. 2, pp. 441–446, Aug. 1978.
- [30] R. O. Jong, J. B. Boffard, L. W. Anderson, and C. C. Lin, "Excitation into  $3p^5 5p$  levels from the metastable levels of Ar," *Phys. Rev. A, Gen. Phys.*, vol. 75, no. 5, p. 052707, May 2007.
- [31] R. S. Schappe, M. B. Schulman, L. W. Anderson, and C. C. Lin, "Measurements of cross sections for electron-impact excitation into the metastable levels of argon and number densities of metastable argon atoms," *Phys. Rev. A, Gen. Phys.*, vol. 50, no. 1, pp. 444–461, Jul. 1994.



**Sergey G. Belostotskiy** was born in Moscow, Russia, in 1983. He received the M.S. degree in plasma physics from Moscow State University, Moscow, Russia, in 2006. Since 2006, he has been working toward the Ph.D. degree with the Department of Chemical and Biomolecular Engineering at the University of Houston, Houston, TX.

His research interests include plasma diagnostics, optical spectroscopy, and physics and chemistry of plasma.



**Vincent M. Donnelly** received the B.A. degree in chemistry from LaSalle University, Philadelphia, PA, and the Ph.D. degree in physical chemistry from the University of Pittsburgh, Pittsburgh, PA.

He is currently a John and Rebecca Moores Professor with the Department of Chemical and Biomolecular Engineering, University of Houston, Houston, TX. Prior to 2002, he was a Distinguished Member of Technical Staff with Bell Laboratories, Murray Hill, NJ. His research includes new nanopatterning methods, experimental studies of plasmas and plasma etching, plasma-surface interactions, and atmospheric pressure microdischarges.

Dr. Donnelly is a member of the American Chemical Society and the American Institute of Chemical Engineers and is a Fellow of the American Vacuum Society.



**Demetre J. Economou** received the Ph.D. degree in chemical engineering from the University of Illinois at Urbana-Champaign, Urbana, in 1986.

Since 1986, he has been with the Department of Chemical and Biomolecular Engineering, University of Houston, Houston, TX, where he is currently a *John and Rebecca Moores Professor* and the Associate Chairman. His research interests include plasma science and technology and nanotechnology.



**Nader Sadeghi** received the M.S. degree in physics and the Doctorat d'Etat es Science Physique for his work on "Kinetics of metastable atoms and charged particles in argon afterglow" from the University of Grenoble, Grenoble, France, in 1964 and 1974, respectively.

In 1965, he was an Assistant Professor with the University of Grenoble. Since 1969, he has been with the Centre National de la Recherche Scientifique (CNRS), where he is currently the Director of Research Emeritus in Laboratoire de Spectrométrie Physique, a joint institute of CNRS and the University of Grenoble. He is the Founder of the Plasma and Reactive Collisions Group, Grenoble University. He was an Invited Professor or Associate Researcher with different universities abroad such as KSU, USA; NDA, Japan; TUE, The Netherlands; and Nagoya, Japan. He was also a Consulting Scientist with AT&T Bell Laboratories, Murray Hill, NJ, and the Centre National d'Etude des Télécommunications, France. His current research interests include plasma diagnostics, plasma chemistry, plasma processing, optical spectroscopy, and collisional processes.